# A unique predator in a unique ecosystem

Montefeitro, Felipe; Lautenschlager, Stephan; Godoy, Pedro; Ferreira, Gabriel; Butler, Richard

*DOI:*
10.1111/joa.13192

SHORT RUNNING PAGE HEADING: MODELLING THE APEX PREDATOR FROM BRAZILIAN LATE CRETACEOUS

# A UNIQUE PREDATOR IN A UNIQUE ECOSYSTEM: MODELLING THE APEX PREDATOR WITHIN A LATE CRETACEOUS CROCODYLIFORM-DOMINATED FAUNA FROM BRAZIL

FELIPE C. MONTEFELTRO[1,2], STEPHAN LAUTENSCHLAGER[2], PEDRO L. GODOY[3], GABRIEL S. FERREIRA[4], RICHARD J. BUTLER[2]

[1]Laboratório de Paleontologia e Evolução de Ilha Solteira, UNESP, Ilha Solteira, Brazil.

[2]School of Geography, Earth and Environmental Sciences, University of Birmingham, Birmingham, UK.

[3]Department of Anatomical Sciences, Stony Brook University, Stony Brook, USA.

[4]Departamento de Biologia, Faculdade de Filosofia, Ciências e Letras de Ribeirão Preto, Universidade de São Paulo, Ribeirão Preto, Brazil.

*felipecmontefeltro@gmail.com*, *s.lautenschlager@bham.ac.uk*, *pedrolorenagodoy@gmail.com*, *gsferreirabio@gmail.com*, *r.butler.1@bham.ac.uk*

ABSTRACT

Theropod dinosaurs were relatively scarce in the Late Cretaceous ecosystems of southeast Brazil. Instead, hypercarnivorous crocodyliforms known as baurusuchids were abundant and probably occupied the ecological role of apex predators. Baurusuchids exhibited a series of morphological adaptations hypothesised to be associated with this ecological role, but quantitative biomechanical analyses of their morphology have so far been lacking. Here, we employ a biomechanical modelling approach, applying finite element analysis (FEA) to models of the skull and mandibles of a baurusuchid specimen. This allows us to characterise the craniomandibular apparatus of baurusuchids, as well as to compare the functional morphology of the group to that of other archosaurian carnivores, such as theropods and crocodylians. Our results support the ecological role of baurusuchids as specialised apex predators in the continental Late Cretaceous ecosystems of South America. With a relatively weak bite force (~600 N), the predation strategies of baurusuchids likely relied on other morphological specializations, such as ziphodont dentition and strong cervical musculature. Comparative assessments of the stress distribution and magnitude of scaled models of other predators (the theropod *Allosaurus fragilis* and the living crocodylian *Alligator mississippiensis*) consistently show different responses to loadings under the same functional scenarios, suggesting distinct predatory behaviors for these animals. The unique selective pressures in the arid to semi-arid Late Cretaceous ecosystems of southeast Brazil, which were dominated by crocodyliforms, possibly drove the emergence and evolution of the biomechanical features seen in baurusuchids, which are distinct from those previously reported for other predatory taxa.

Keywords: Finite Element Analysis; Baurusuchidae; Notosuchia

## INTRODUCTION

In nearly all known continental Cretaceous ecosystems worldwide, the dominant hypercarnivores and apex predators were theropod dinosaurs (Lloyd et al. 2008; Benson et al. 2013; Zanno & Mackovicky 2013). However, in the Late Cretaceous ecosystems of Brazil, theropods were exceptionally scarce. Instead, the putative dominant apex predators were a group of large, terrestrial crocodyliforms, the baurusuchids (Riff & Kellner 2011; Godoy et al. 2014). Baurusuchids are phylogenetically included within Notosuchia, a group of highly diverse crocodyliforms which thrived mainly in Gondwana during the Cretaceous (Pol & Leardi 2015; Mannion et al. 2015). Exhibiting a wide range of morphological variation, from gracile omnivores to pug-nosed herbivores, notosuchians significantly contributed to the highest peak of morphological disparity experienced by crocodyliforms across their evolutionary history (Wilberg 2017; Godoy et al. 2019; Melstrom & Irmis 2019; Godoy 2020).

Although present in other parts of Gondwana, most baurusuchid species (ca. 80%) are found in the Late Cretaceous rocks of the Bauru Group, in southeast Brazil (Carvalho et al. 2005; Godoy et al. 2014; Montefeltro et al. 2011). The Bauru Group palaeoecosystem witnessed an extraordinary abundance of notosuchians, with nearly 30 species described so far. While dinosaurs were also present, their fossil record in this rock sequence is relatively poor (Montefeltro et al. 2011; Godoy et al. 2014). Within this crocodyliform-dominated ecosystem, baurusuchids are the likely apex predators. Baurusuchids exhibited a series of morphological adaptations hypothesised to be associated with their role as terrestrial hypercarnivores, possibly achieved via heterochronic transformations, such as hypertrophied canines, a reduced number of teeth, and dorsoventrally high skulls (Montefeltro et al. 2011; Riff & Kellner 2011; Godoy et al. 2018; Wilberg et al. 2019). However, quantitative assessments of the

palaeobiology of baurusuchids are lacking, and the data supporting their role as apex predators is primarily derived from broad generalizations and the faunal composition of the Bauru palaeoecosystem (Riff & Kellner 2011; Godoy et al. 2014).

Here, we employ a biomechanical modelling approach in a comparative investigation of the functional morphology of a baurusuchid (*Baurusuchus*), one analogue of a possible ecological competitor (*Allosaurus*), and an extant crocodyliform (*Alligator*). Using finite element analysis (FEA), we characterize the baurusuchid skull biomechanically and quantify functional similarities and differences between baurusuchids, theropod dinosaurs and living crocodylians. We also calculate bite forces, simulate functional scenarios, and conduct bending tests to reveal biomechanical properties of the baurusuchid skull. Our results shed light on key biomechanical aspects that may have allowed this group to dominated the unique ecosystems present during the Cretaceous in Brazil.

## METHODS

**Specimens.** The baurusuchid specimen modelled for the present study is a complete skull with lower jaws, referred to *Baurusuchus pachecoi* (LPRP/USP 0697 Laboratório de Paleontologia USP-RP, Figure 1-A) and collected in Jales, Brazil (Adamantina Formation, Bauru Group; Montefeltro 2019). *Baurusuchus* is a typical baurusuchid, presenting the set of anatomical traits that characterizes Baurusuchidae and therefore being representative of the clade as a whole (Montefeltro et al. 2011, Godoy et al. 2014). The specimen used for this study has a basal skull length of 33.10 cm (see Table 1 for more cranial measurements), and an estimated total body length of approximately 170 cm, based on the preserved portions of the skeleton (Montefeltro 2019). Compared

to other relatively complete skeletons of adult baurusuchids, such as *Aplestosuchus sordidus* and *Baurusuchus albertoi*, the specimen LPRP/USP 0697 represents a medium-sized baurusuchid (Godoy et al. 2016), with the basal skull length being 70% of that of the holotype of *Stratiotosuchus maxhechti* (one of the largest complete skulls known among baurusuchids: Riff & Kellner, 2011; Godoy et al. 2016).

For comparison, we modelled a specimen of the theropod dinosaur *Allosaurus fragilis* (MOR 693, Museum of the Rockies, Bozeman, Figure 1-B) and one specimen of *Alligator mississippiensis* (OUVC 9761, Ohio University Vertebrate Collections, Figure 1-C) (see Rayfield et al. 2001, Witmer & Ridgely 2008 for scanning details). *Allosaurus fragilis* was chosen based on its medium size when compared to other theropods, which is equivalent to the putative size of the theropods from the Adamantina Formation, for which no complete craniomandibular material is currently known. Furthermore, *Allosaurus* has been proposed to be functionally similar to abelisaurids, the most commonly found theropods in the Bauru Group (Sakamoto 2010). The choice of *Alligator mississippiensis* (as a living representative of the crocodyliform lineage) was made because this is a model organism for herpetological and functional studies (Guillette et al. 2007; Farmer & Sanders 2010; Reed et al. 2011). For the subsequent FEA, existing 3D models of *Allosaurus fragilis* and *Alligator mississippiensis* from previous studies were used (Rayfield et al. 2001; Witmer & Ridgely 2008; Lautenschlager 2015). The *Baurusuchus pachecoi* skull was scanned in a Toshiba Aquilion Prime machine, at “Hospital das Clínicas de Ribeirão Preto”, Brazil. The scan resulted in 1917 projections, generating 1,187 slices (thickness of 0.5 cm), voltage of 120 kV, and current of 150 μA. The segmentation of bones was performed with Amira 5.3 (Thermo Fisher Scientific).

**FEA.** The 3D models of all specimens, including skulls and mandibles, were imported into Hypermesh 11 (Altair Engineering) for the generation of solid tetrahedral meshes (consisting of approximately 1,000,000 elements per model). For the *Alligator* and the baurusuchid models, material properties for bone and teeth were assigned based on values for *Alligator mississippiensis* (bone: E = 15.0 GPa, υ = 0.29, teeth: E = 60.4 GPa, υ = 0.31; Porro et al. 2011; Sellers et al. 2017), whereas for the *Allosaurus* model, values were derived from studies on theropods (bone: E = 20.0 GPa, υ = 0.38, teeth: E = 60.4 GPa, υ = 0.31; Rayfield et al. 2001, 2011). To exclude the possibility of different results due to distinct material properties we also conducted an FEA on the *Allosaurus* model using the same bone and teeth properties assigned to the crocodyliform models. All material properties in the models were assigned in Hypermesh and treated as isotropic and homogeneous.

Intrinsic scenarios for the baurusuchid, *Allosaurus fragilis* and *Alligator mississippiensis*, were simulated for the skull and lower jaw models, using a simplified jaw adductor muscle-driven biting. The adductor muscle forces of the baurusuchid were estimated using the attachment area for each muscle (Figure 2), based on previous works on extant and extinct crocodyliforms (Holliday & Witmer 2009; Holliday et al. 2013). The adductor chamber reconstruction of the dinosaur and crocodylian was based on previously published data for the muscle arrangements for both taxa (Rayfield et al. 2001, 2011; Porro et al. 2011; Sellers et al. 2017). The attachment areas measured for the three taxa were used as a proxy for physiological cross-section area, which was then multiplied by an isometric muscle stress value of 25.0 N/cm$^2$ (Porro et al. 2011). Table 2 shows the total muscle force inferred for each muscle. Although this isometric muscle stress is on the lower margin of the range of values reported for vertebrate muscles (e.g. 32N/cm$^2$ and 35N/cm$^2$) it was selected here due to the relatively close phylogenetic

position of baurusuchids to modern crocodilians. However, the calculated bite force would be only slightly (10-15%) higher using different values for isometric muscle stress. Three intrinsic scenarios were analysed to estimate the muscle-driven biting force in the baurusuchid, (1) a bilateral bite at the second maxillary and the fourth dentary tooth, (2) a unilateral bite at the second maxillary and the fourth dentary tooth, and (3) unilateral bite at the third premaxillary tooth. One intrinsic scenario was analysed for both *Allosaurus fragilis* and *Alligator mississippiensis*: the maxillary and dentary unilateral bite scenarios. For each intrinsic scenario in all taxa, constraints were placed on nodes at the craniomandibular articular surfaces. Each node was constrained in all directions (x, y, z). For the skulls, three nodes were constrained on the occipital condyle, and two nodes on each quadrate articular surface. For the lower jaws, three (baurusuchid) or four (*Allosaurus* and *Alligator*) nodes on each glenoid were constrained. To estimate the biting force of the baurusuchid, nodes were constrained at the tip of the teeth to measure the reaction force caused by the modelled adductor muscles and the same approach was used for the other two taxa. In unilateral scenarios, the tip of one tooth was constrained, while in bilateral scenarios the tip of the teeth on both sides was constrained. For the baurusuchid, the constrained teeth were PM3, M2 and D4; for *Allosaurus fragilis*, M3 and D5; for *Alligator mississippiensis*, M4 and D4. The intrinsic scenarios were all based on the same jaw adductor reconstructions for each taxon, and aimed to emulate possible behaviours of baurusuchids, theropod dinosaurs and crocodylians.

To investigate the craniomandibular biomechanical properties in alternative load assignments, five bending scenarios were also tested for the baurusuchid skull and mandible models: unilateral bending, bilateral bending, pull-back, head-shake, and head-twist. The bending test scenarios were proposed as an additional investigation of

the skull properties in situations that approach behaviours during different types of strikes, including biting (unilateral bending and bilateral bending) and supplementary head movements allowed by postcranial musculature (pull-back, head-shake, and head-twist). The loading applied for each scenario was based on the approximation of the greatest bite force obtained from the intrinsic scenario (600 N; see results below). All loadings in the unilateral bending scenario were applied to one node, perpendicular to the occlusal planes on one of the following teeth: D1, D4, D9, PM2, PM3, M2 and M4. Bilateral bending scenarios were tested with the same conditions as the unilateral ones, but with two vectors of 300 N applied symmetrically to each canine at the M4 and the D4. The head-shake scenario was tested with two vectors of 300 N pointing to the same direction, one on one node on the labial surface of left M2/D4 and the other on one node on the lingual surface of right M2/D4. For the pull-back, the load force of 600 N was applied to one node at crown midheight over the distal carina of the caniniform teeth (D4, PM3 and M2). For the head twist, the loadings were applied to two opposite vectors of 300 N in each model. One loading vector was applied to one node at the tip of the maxillary (M2) or dentary (D4) caniniform tooth, and another loading vector on the opposite side on the dorsal surface of the maxilla, or ventral surface of the dentary respectively.

Four bending scenarios were also tested in the skull and lower jaws of *Allosaurus fragilis* and *Alligator mississippiensis*, for comparison. Unilateral and bilateral bending were simulated to the comparable positions of the tested in the baurusuchid. Unilateral bending was tested in PM2, M3, M16, D1, D4 and D13 for *Allosaurus fragilis*, and PM2, M4, M15, D2, D4 and D15 for *Alligator mississippiensis*. Bilateral bending was also tested in M3 and D5 pairs for the theropod, and M4 and D4 pairs for the crocodylian. For meaningful comparisons of form and function

independent of size (Dumont et al., 2009), all models used in the bending tests were scaled to the total surface of the baurusuchid specimen. For the bending scenarios, constraints were placed on the same nodes as in the intrinsic scenarios. The performances for the FEA models were assessed via contour plots of von Mises stress distribution and mean von Mises stress and displacement values per element. To avoid the influence of individual stress singularities, such as at the constrained or loaded nodes, we used an averaging threshold of 99%.

## RESULTS

During the bilateral bite scenario, the bite force estimate for the baurusuchid specimen was 252 N for the skull and 578 N for the lower jaw. For the premaxillary unilateral bite scenario, bite force was estimated as 199 N, whereas for both maxillary and lower jaw unilateral bite scenarios, it was 450 N. The distribution and magnitude of the von Mises stress showed little difference in the intrinsic scenarios for the skull and lower jaw of the baurusuchid (Figure 3). Most of the elements in the skull remained relatively stress-free in the three intrinsic scenarios simulated (mean von Mises stress of 0.46 MPa during the bilateral maxillary biting, 0.50 MPa during the unilateral maxillary biting, and 0.52 MPa during the premaxillary unilateral biting). The quadrate body, the body of the ectopterygoid, and the posterior margin of the pterygoid are the main regions in which stresses are present during those simulated scenarios (Figure 3). In the intrinsic scenario for the premaxillary canine bite, there is also increased stress at the anterior margin of the notch between the premaxilla and maxilla, which also extends medially surrounding the notch at the secondary bony palate. As expected, the lower jaws experienced more von Mises stress than the skull model (mean von Mises stress of 1.93

MPa in the bilateral biting, and 2.01 MPa in the unilateral biting). In both scenarios, the symphyseal region surrounding the canine teeth, and the retroarticular process remained relatively stress-free, and the greatest von Mises stress is observed on the dorsal surface of the surangular and ventral surface of the angular.

Considerable differences were found between the von Mises stress magnitudes of the skull and lower jaws of the baurusuchid among the different bending scenarios tested (e.g. mean values of 0.4 MPa in the skull head twist and of 24.7 MPa in the bilateral biting of the lower jaws). Although variable in magnitude, a general pattern is discernable in the stress distribution in the skull and lower jaws of the baurusuchid (Figure 4). The greatest von Mises stresses in the skull models are mostly present in the posterior and median portions of the skull, with stress hotspots located on the ventral and lateral regions of the quadrate body, ventral region of the infratemporal bar, and preorbital region (anterior jugal, posterior maxillae, lacrimals, nasal, prefrontals, and anterior frontal). In addition, the areas of maximum von Mises stress in the premaxillae and maxillae are isolated from each other. This means that when loading is applied to the premaxillary teeth, the maxillae remain relatively stress-free, whereas the dorsal rostrum (premaxilla and nasals) is more stressed. When loading is applied to the maxillary teeth, the premaxillae remain unstressed, and stress is concentrated on the posterior portion of the skull (Figure 4).

The lower jaws also experienced more von Mises stress than the skull model during the bending tests, and the stress hotspots are more homogeneously distributed, located on the dorsal surface of the surangular, angular and retroarticular process. Two exceptions are the jaw pull-back scenario, in which the stress hotspots are located around the mandibular fenestra; and the bilateral bending scenario, in which most of the lower jaw is highly stressed, and only the symphyseal region remains less stressed.

The areas around the maxillary and dentary canines remain relatively stress-free, even during scenarios in which the loadings were applied to the canines (both in the intrinsic scenarios and the bending tests). This is particularly evident for the dentary canine, for which the surrounding bone remains unstressed in all scenarios, including the least optimal scenario of the bilateral bending (Figure 4).

In general, the patterns of von Mises stress distribution obtained for *Allosaurus* and *Alligator* (Figure 5 and Figure 6) were consistent with previous studies (Rayfield et al. 2001; Porro et al. 2011). Even considering that the bone properties assigned to the *Allosaurus* are slightly different from the other models, it did not substantially change the results obtained from this taxon. Considering the intrinsic scenarios, the measured mean von Mises stress is similar during maxillary unilateral biting (mean von Mises stress of 0.72 MPa for *Allosaurus* and 0.62 MPa for *Alligator*). The pattern of stress distribution observed in the models of the *Alligator* are much closer to the observed in the baurusuchid than to the *Allosaurus*, perhaps related to the phylogenetic proximity reflected in the cranial architecture of both crocodyliforms.

The two taxa retrieved greater differences in the lower jaw models during the intrinsic scenarios (mean von Mises stress of 3.7 MPa for *Allosaurus* and 0.99 MPa for *Alligator*). The discrepancies observed in the bending scenarios are also most evident in the lower jaws, which for the baurusuchid remain consistently less stressed than those of both the theropod and the crocodylian during the bending tests. When compared to the baurusuchid, the theropod models obtained only slightly lower mean von Mises stress values for the skull, but much higher values for the lower jaws (Figure 6). The alligator model, in contrast, retrieved higher mean von Mises stress values in most scenarios than both the baurusuchid and *Allosaurus*, even though differences in stress values are less distinguishable between skull models of the analysed taxa (Figure 6).

The only scenario that does not follow this pattern is the unilateral bending at the back of the upper tooth row, in which the mean von Mises stress value is similar for the baurusuchid and *Alligator*, although both have higher stresses than the theropod. The most divergent results are related to the mandibular anterior bending scenario, in which the mean stress value in *Alligator* was more than nine times higher than in the baurusuchid, and almost twice the mean von Mises stress recorded for the theropod.

## DISCUSSION

The unexpectedly weak bite force estimated for the baurusuchid is much lower than that measured for extant crocodylians of comparable size. For example, *Alligator sinensis* has a similar total body length (150–200 cm) and can have a bite of up to 963 N (measured at the caniniform tooth), whereas *Paleosuchus* is the only living species with comparable bite force values (Erickson et al. 2012). The bite force estimated for the baurusuchid is also only a fraction of the bite forces inferred for adult theropods, which could potentially exceed 50,000 N (Gignac & Erickson 2017). Furthermore, in order to estimate the bite force of extinct crocodyliforms, previous studies have applied equations based on regression data from extant crocodylians (e.g. Aureliano et al. 2015). Although, this type of equation is likely to relatively correctly estimate the bite force for fossil crocodyliforms phylogenetically close to the Crocodylia clade and sharing the basic cranial architecture, it does not take into consideration the very different cranial architectures present in more distantly related taxa, such as baurusuchids. As a result, this equation may not be accurate for anatomically divergent taxa, and will overestimate or underestimate the bite forces of those taxa. We applied the equations presented by Aureliano et al. (2015), which uses data from living species (Verdade 2000; Erickson et

al. 2012), to the craniomandibular measurements of the specimen studied here (LPRP/USP 0697) and obtained a much higher bite force estimation (of nearly 4,000 N). This apparent overestimation demonstrates that the differences between the cranial structures of living and extinct crocodyliforms may have important functional implications, such as the disproportionately positive bite force increase previously inferred for baurusuchids (Gignac & O'Brien 2016).

In this context, it is noteworthy that the bite force estimates from FEA vary when using the skull or the mandible to obtain reaction forces. This is not surprising as the geometry and architecture of the skull is more complex and subject to further constraints than in the mandible. Validation tests have shown, however, that realistic bite forces can be estimated from mandible models (Porro et al. 2011). Consequently, we consider the higher bite force values obtained from the mandible as the more likely for the baurusuchid.

This comparatively weak bite force in baurusuchids suggests that their role as apex predators may have involved hunting strategies different from those of most carnivorous theropods and living crocodylians, which mostly rely on muscle-driven biting forces for killing (Rayfield 2004, 2005, 2011; D´Amore et al. 2011; Erickson et al. 2012). As a consequence, the killing potential of baurusuchids could have been enhanced by structural and behavioural traits, as in other weak-bite apex predators such as troodontid and allosaurid theropods, varanid lizards, and felines, all of which harness the postcranial musculature to supplement bite force (Rayfield 2001; D´Amore et al. 2011; Figueirido et al. 2018; Torices et al. 2018).

Alternatively, the apex predator role of baurusuchids could have been a historical misinterpretation, and the group might be better interpreted as preying on

317 smaller and/or softer animals. However, a series of craniomandibular and postcranial
318 adaptations of baurusuchids indicate otherwise. For example, the presence of extensive
319 overengineered regions around the canines in both the skull and lower jaws (e.g. regions
320 that remain relatively stress-free in all tests) show that the baurusuchid
321 craniomandibular architecture could safely perform in much higher stress conditions
322 than imposed by muscle-driving biting forces. This is true even for our bending tests
323 that most likely overestimate the stress experienced by the skull of the baurusuchid. The
324 presence of overengineered regions in *Allosaurus* has been suggested as evidence that
325 this taxon also used mechanisms to enhance killing potential in its regular feeding
326 strategy (Rayfield et al. 2001).

327 Additionally, the tested pull-back, head-shake and head-twist scenarios were
328 designed to understand how the baurusuchid craniomandibular architecture would
329 perform during similar head movements employed by other weak- and strong-bite apex
330 predators (Rayfield 2001; D´Amore et al. 2011; Torices et al. 2018). For baurusuchids,
331 these movements would be possible given the robust cervical vertebrae, high neural
332 spines, and well-developed cervical ribs (particularly the first two), which provided
333 large attachment areas for the muscles responsible for head lift, head twist, and side-to-
334 side movements (Cleuren & De Vree 2000; Godoy et al. 2018). These tests show that
335 the baurusuchid skull and mandible worked optimally in scenarios simulating non-
336 orthal loads, suggesting that baurusuchids were well-suited for head movements during
337 predation, possibly even more so than living crocodylians. This can be explained by the
338 combination of three skull features that minimize skull stress during bites and torsion,
339 the oreinirostral morphology, the absence of the antorbital fenestra, and the extensively
340 ossified secondary palate. This combination of features is particularly efficient for stress
341 reduction during unilateral biting (Rayfield & Milner 2008).

Our tests also revealed that the well-developed gap between premaxillae and maxillae is a unique specialization in the skull architecture of baurusuchids, very likely related to predatory habits. This gap redirects the stress from the premaxillae to the dorsal surface of the fused nasals during biting, preventing stress from traveling from the occlusal region of one bone to the other, and implying a functional decoupling between premaxillae and maxillae during bites. This gap at the premaxillae-maxillae suture is absent in *Allosaurus* and *Alligator*, and in those taxa, the stress travels directly from the premaxilla to the maxilla, especially during the unilateral premaxillary bending scenarios. A similar stress redirection is observed in tyrannosaurids, in which the robust and also fused nasals work as the main route for stress distribution, bypassing the less robust maxilla-lacrimal contact (Rayfield 2005). We suggest that the gap observed in baurusuchids, in combination with the robust and fused nasals, worked similarly to that of tyrannosaurids, even though, the general cranial architecture presented by the baurusuchid is closer to the *Alligator*. The gap could also allow repeated punctures to be inflicted from biting at different positions of the tooth row, but concomitantly working as a built-in safety factor, minimizing the risk of the skull yielding (Rayfield et al., 2001). Finally, the presence of ziphodont dentition in baurusuchids is also in line with the role of apex predator (Riff & Kellner 2011; Godoy et al. 2014). Knife-like teeth with well-developed serrated cutting edges are a dental adaptation for optimal defleshing of vertebrate carcasses (D´Amore et al. 2009) and are present in a series of unrelated apex predators, including theropod dinosaurs and large monitor lizards (D´Amore et al. 2011; Brink & Reisz 2014; Torices et al. 2018).

The discrepancy in the von Mises stress magnitude and distribution seen between the mandibles of the three taxa during the intrinsic scenarios and during the bending tests suggests that this structure is also pivotal in understanding the

palaeoecology of baurusuchids. The von Mises stress distribution shows that *Allosaurus* and *Alligator* have, in general, higher and more homogeneously distributed von Mises stress in the mandible, while in the baurusuchid the stress is concentrated at the postsymphyseal region. This indicates that the robust symphysis in baurusuchids is important for stabilizing the lower jaws.

The best example of the divergent responses among lower jaws is seen in the bilateral bending scenario, for which the mean von Mises stress value for the baurusuchid was approximately five times greater than any other scenario. Additionally, this is the only scenario in which the von Mises stress approaches the higher values presented by *Allosaurus* and *Alligator* (Figure 6). The baurusuchid response is also different from *Allosaurus* and *Alligator* in the sense that the mean von Mises stress values in the bilateral bending scenarios are distinct from the unilateral scenarios, whereas the other two taxa show similar values in both scenarios. Based on our FEA results, we propose that the bilateral biting is the least likely killing strategy for baurusuchids, and the clamp-and-hold, employed by living crocodylians, and large mammal predators, such as the lion (*Panthera leo*) (Figueirido et al. 2018), does not fit the mechanical properties of the baurusuchid skull.

Our results also indicate that baurusuchids were well adapted for handling struggling prey, which was possibly subdued by inflicting a series of bites using premaxillary, maxillary and particularly the dentary canines, that combined with ziphodonty would pierce repeatedly the skin of the prey. The puncture phase would be followed by head-movements that would worsen the wounds caused by the punctures and ultimately leading to the death of the prey.

Our results successfully characterise the exceptional suite of biomechanical properties displayed by baurusuchids, which combine novel adaptations, features similar to theropods, and others seen in living crocodylians. Such a combination has not been reported previously for any predatory taxon, raising questions on the specific evolutionary settings that allowed these features to emerge. Selective pressures from extrinsic environmental factors seem to have an important influence during amniote functional and biomechanical evolution (Sakamoto et al. 2019). In the case of baurusuchids, the unique Late Cretaceous palaeoecosystems of southeast Brazil exhibited a combination of playa-lake systems and transitory rivers which possibly permitted life to flourish in semi-arid to arid conditions (Carvalho et al. 2010; Marsola et al. 2016). These landmasses witnessed an extraordinary diversity of crocodyliforms (especially notosuchians; Mannion et al. 2015), as well as other tetrapods (Godoy et al. 2014). This resulted in a diverse array of potential prey for baurusuchids among terrestrial tetrapods, including crocodyliforms and sauropods, indicating that prey selection could have played an important role in the evolution of the baurusuchid craniomandibular apparatus.



## ACKNOWLEDGEMENTS

This work was supported in part by a Rutherford Fund Strategic Partner Grant to the University of Birmingham, which funded the travel of FCM to Birmingham. This research was supported by a National Science Foundation grant (NSF DEB 1754596) to PLG and Fundação de Amparo à Pesquisa do Estado de São Paulo (FAPESP 2019/10620-2) to GSF. We thank two reviewers for their comments which improved the final version of this manuscript.

414

415 AUTHOR CONTRIBUTIONS

416 FCM, SL, and RJB conceived and designed the experiments. FCM, SL, PLG, GSF and
417 RJB analyzed the data. FCM, SL, and PLG wrote the paper. All authors read,
418 commented on and approved the final version of the article.

419

420 REFERENCES


421 Aureliano T, Ghilardi AM, Guilherme E, Souza-Filho JP, Cavalcanti M, Riff D (2015)
422 Morphometry, bite-force, and paleobiology of the Late Miocene Caiman
423 Purussaurus brasiliensis. *PLOS ONE*, **10,** e0117944.

424 Benson RBJ, Mannion PD, Butler RJ, Upchurch P, Goswami A, Evans SE (2013)
425 Cretaceous tetrapod fossil record sampling and faunal turnover: implications for
426 biogeography and the rise of modern clades. *Palaeogeogr Palaeoclimatol*
427 *Palaeoecol*, **372,** 88–107.

428 Brink KS, Reisz RR (2014) Hidden dental diversity in the oldest terrestrial apex
429 predator *Dimetrodon*. *Nat Commun*, **5,** 3269.

430 Carvalho IS, Campos ACA Nobre PH (2005) *Baurusuchus salgadoensis,* a new
431 Crocodylomorpha from the Bauru Basin (Cretaceous), Brazil. *Gondwana Res*, **8,**
432 11–30.

433 Carvalho IS, Gasparini ZB, Salgado L, Vasconcellos FM, Marinho TS (2010) Climate's
434 role in the distribution of the Cretaceous terrestrial Crocodyliformes throughout
435 Gondwana. *Palaeogeogr Palaeoclimatol Palaeoecol*, **297,** 252–262.

436 Cleuren J, De Vree F (2000) Feeding in Crocodilians. In: *Feeding: form, function and*
437 *evolution in tetrapod vertebrates* (ed. Schwenk K), pp. 337–358, San Diego:
438 Academic Press.

439 D´Amore DC (2009) A functional explanation for denticulation in theropod dinosaur
440 teeth. *Anat Rec*, **292,** 1297–1314.

441 D´Amore DC, Moreno K, McHenry CR, Wroe S (2011) The effects of biting and
442 pulling on the forces generated during feeding in the Komodo dragon (*Varanus*
443 *komodoensis*). *PLOS ONE*, **6,** e26226.

444 Dumont E, Grosse I, Slater G (2009) Requirements for comparing the performance of
445 finite element models of biological structures. *J Theor Biol,* **256,** 96–103.

446 Erickson G, Gignac P, Steppan S, et al. (2012) Insights into the ecology and
447 evolutionary success of crocodilians revealed through bite-force and tooth-
448 pressure experimentation. *PLOS ONE,* **7,** e31781.

449 Farmer CG, Sanders K (2010) Unidirectional airflow in the lungs of alligators. *Science*,
450 **327,** 338–340.

451 Figueirido B, Lautenschlager S, Pérez-Ramos A, Valkenburgh B (2018) Distinct
452 predatory behaviors in scimitar- and dirk-toothed sabertooth cats. *Curr Bio*, **28,**
453 3260–3266.

454 Gignac P, O'Brien H (2016) Suchian feeding success at the interface of ontogeny and
455 macroevolution. *Integr Comp Biol*, **56,** 449–458.

456 Gignac P, Erickson G (2017) The Biomechanics behind Extreme Osteophagy in
457 *Tyrannosaurus rex*. *Sci Rep*, **7,** 2012.

458 Godoy PL (2020) Crocodylomorph cranial shape evolution and its relationship with
459 body size and ecology. *J Evol Biol*, 33, 4–21.

460 Godoy PL, Montefeltro FC, Norell MA, Langer MC (2014) An additional baurusuchid
461 from the cretaceous of Brazil with evidence of interspecific predation among
462 crocodyliformes. *PLOS ONE,* **9,** e97138.

463 Godoy PL, Bronzati M, Eltink E, et al. (2016) Postcranial anatomy of *Pissarrachampsa*
464 *sera* (Crocodyliformes, Baurusuchidae) from the Late Cretaceous of Brazil:
465 insights on lifestyle and phylogenetic significance. *PeerJ*, **4,** e2075.

466 Godoy PL, Benson RBJ, Bronzati M, Butler R (2019) The multi-peak adaptive
467 landscape of crocodylomorph body size evolution. *BMC Evol Biol,* **19,** 167.

468 Godoy PL, Ferreira G, Montefeltro FC, Vila Nova BC, Butler RJ, LangerMC (2018)
469 Evidence for heterochrony in the cranial evolution of fossil crocodyliforms.
470 *Palaeontology,* **61,** 543–558.

471 Guillette Jr LJ, Edwards TM, Moore BC (2007) Alligators, contaminants and steroid
472 hormones. *Environ Sci*, **14,** 331–347.

473 Holliday C, Witmer LW (2009) The epipterygoid of crocodyliforms and its significance
474 for the evolution of the orbitotemporal region of eusuchians. *J Vert Paleontol*,
475 **29,** 715–733.

476 Holliday C, Tsai H, Skiljan R, George I, Pathan S (2013) A 3D interactive model and
477 atlas of the jaw musculature of *Alligator mississippiensis*. *PLOS ONE,* **8,**
478 e62806.

479 Lautenschlager S (2015). Estimating cranial musculoskeletal constraints in theropod
480 dinosaurs. *R Soc Open Sci*, **2,** 150495

481 Lloyd GT, Davis KE, Pisani D, et al. (2008). Dinosaurs and the Cretaceous terrestrial
482 revolution. *Proc R Soc B*, **275,** 2483–2490.

483 Mannion P, Benson R, Carrano M, Tennant J, Judd J, Butler R (2015). Climate
484 constrains the evolutionary history and biodiversity of crocodylians. *Nat*
485 *Commun,* **6,** 8438.

486 Marsola, J. C. A., Batezelli, A., Montefeltro, F. C., Grellet-Tinner, G. & Langer, M. C.
487 (2016). Palaeoenvironmental characterization of a crocodilian nesting site from
488 the Late Cretaceous of Brazil and the evolution of crocodyliform nesting
489 strategies. *Palaeogeogr Palaeoclimatol Palaeoecol*, **457,** 221–232.

490 Melstrom KM, Irmis RB (2019) Repeated evolution of herbivorous crocodyliforms
491 during the Age of Dinosaurs. *Curr Bio*, **29,** 2389–2395.

492 Montefeltro FC (2019). The osteoderms of baurusuchid crocodyliforms
493 (Mesoeucrocodylia, Notosuchia). *J Vert Paleontol*. e1594242.

494 Montefeltro FC, Larsson HCE, Langer MC (2011) A new baurusuchid
495 (Crocodyliformes, Mesoeucrocodylia) from the late cretaceous of Brazil and the
496 phylogeny of Baurusuchidae. *PLOS ONE,* **6,** e21916.

Pol D, Leardi J (2015) Diversity patterns of Notosuchia (Crocodyliformes, Mesoeucrocodylia) during the Cretaceous of Gondwana. In: *Reptiles Extintos – Volumen en Homenaje a Zulma Gasparini* (ed. Fernández M, Herrera Y), pp. 172–186, Buenos Aires: Publicación Electrónica de la Asociación Paleontológica Argentina.

Porro L, Holliday C, Anapol F, Ontiveros L, Ontiveros L, Ross C (2011) Free body analysis, beam mechanics, and finite element modeling of the mandible of *Alligator mississippiensis*. *J of Morphol,* **272,** 910–937.

Rayfield E (2004) Cranial mechanics and feeding in *Tyrannosaurus rex*. *Proc R Soc B*, **271,** 1451–1459.

Rayfield E (2005) Aspects of comparative cranial mechanics in the theropod dinosaurs *Coelophysis, Allosaurus* and *Tyrannosaurus*. *Zool J Lin Soc*, **144,** 309–316.

Rayfield E (2011) Structural performance of tetanuran theropod skulls, with emphasis on the Megalosauridae, Spinosauridae and Carcharodontosauridae. *Spec Pap Palaeontol*, **86,** 241–253.

Rayfield E, Norman DB, Horner CC, et al. (2001) Cranial design and function in a large theropod dinosaur. *Nature*, **409,** 1033–1037.

Rayfield E, Milner A (2008) Establishing a framework for archosaur cranial mechanics. *Paleobiology*, **34,** 494–515.

Reed DA, Porro LB, Iriarte-Diaz J, et al. (2011) The impact of bone and suture material properties on mandibular function in *Alligator mississippiensis*: testing theoretical phenotypes with finite element analysis. *J Anato*, **218,** 59–74.

Riff D, Kellner A (2011) Baurusuchid crocodyliforms as theropod mimics: Clues from the skull and appendicular morphology of *Stratiotosuchus maxhechti* (Upper Cretaceous of Brazil). *Zool J Lin Soc,* **163(suppl_1)**, S37–S56.

Sakamoto M (2010) Jaw biomechanics and the evolution of biting performance in theropod dinosaurs. *Proc R Soc B,* **277,** 3327–3333.

Sakamoto M, Ruta M, Venditti C (2019) Extreme and rapid bursts of functional adaptations shape bite force in amniotes. *Proc R Soc B*, **286,** 20181932.

Sellers K, Middleton K, Davis J, Holliday C (2017) Ontogeny of bite force in a validated biomechanical model of the American alligator. *J Exp Biol,* **220,** 2036–2046.

Torices A, Wilkinson R, Arbour VM, Ruiz-Omenaca JI, Currie PJ (2018) Puncture-and-pull biomechanics in the teeth of predatory coelurosaurian dinosaurs. *Curr Bio*, **28,** 1467–1474.

Verdade LM (2000) Regression equations between body and head measurements in the broad-snouted caiman (*Caiman latirostris*). *Rev Bras Biol*, **60,** 469–482.

Wilberg EW (2017) Investigating patterns of crocodyliform cranial disparity through the Mesozoic and Cenozoic. *Zool J Lin Soc*, **181,** 189–208.

536 Wilberg EW, Turner AH, Brochu CA (2019) Evolutionary structure and timing of
537 major habitat shifts in Crocodylomorpha. *Sci Rep*, **9,** 1–10.

538 Witmer L, Ridgely R (2008) The paranasal air sinuses of predatory and armored
539 dinosaurs (Archosauria: Theropoda and ankylosauria) and their contribution to
540 cephalic structure. *Anat Rec,* **291,** 1362–1388.

541 Zanno L, Makovicky P (2013) Neovenatorid theropods are apex predators in the Late
542 Cretaceous of North America. *Nat Commun,* **4,** 2827.

543

FIGURE LEGENDS

**Figure 1.** Digitally restored models of skulls used in this study. A- Baurusuchid (LPRP/USP 0697) in lateral view showing typical traits of the members of the clade. B- *Allosaurus fragilis* (MOR 693) in lateral view. C- *Alligator mississippiensis* (OUVC 9761) in lateral view.

**Figure 2.** Muscle attachment areas plotted on the 3D model of skull the baurusuchid LPRP/USP 0697. A, skull and lower jaws in lateral view; B, dorsal view of the left posterior of the skull; C, ventral view of the left posterior of the skull; D, posterolateral view of the skull; E, occipital view of the left portion of the skull; F, lateral view of the posterior portion of the left mandibular ramus; G, medial view of the posterior portion of the left mandibular ramus; H, occlusal view of the posterior portion of the left mandibular ramus; I, ventral view of the posterior portion of the left mandibular ramus. **MAMEM**: *m. adductor mandibulae externus medialis*; **MAMEP**: *m. adductor mandibulae externus profundus*; **MAMES**: *m. adductor mandibulae externus superficialis*; **MAMP**: *m. adductor mandibulae posterior*; **MDM**: *m. depressor mandibulae*; **MIRA**: *m. intramandibularis*; **MPSTPS**: *m. pseudotemporalis profundus*; **MPTD**: *m. pterygoideus dorsalis*; **MPTV**: *m. pterygoideus ventralis*.

**Figure 3.** Von Mises stress contour plots from finite elements analysis (FEA) of the baurusuchid specimen (LPRP/USP 0697) for the intrinsic scenarios. Arrows indicate the location of muscle-driven bite forces on models during each scenario, with respective estimated bite force values. Mean von Mises values per scenario are displayed on the bottom right. **JBMB.**: jaw bilateral mucle-driven bite; **JUMB.**: jaw unilateral mucle-driven bite; **SBMB.**: skull bilateral muscle-driven bite; **SUMB.**; skull unilateral muscle-driven bite; **UPMB.**: unilateral premaxillary muscle-driven bite.

**Figure 4.** Von Mises stress contour plots from FEA of the baurusuchid specimen LPRP/USP 0697, comparing the stress distribution of skull and mandible models under distinct functional bending scenarios. Arrows indicate the location on the models of the

574 loading vectors for each scenario. Mean von Mises values per scenario are displayed on
575 the bottom right. **D.1**: jaw anterior unilateral bending; **D.4**: jaw canine unilateral
576 bending; **D.PB.**: dentary canine pull-back; **D.S.**: canine dentary shake; **HT.**: head-twist
577 (skull); **JBB.**: jaw canine bilateral bending; **JT.**: head-twist (jaw); **M.2**: maxilla canine
578 unilateral bending; **M.4**: maxilla posterior unilateral bending; **MBB.**: maxilla canine
579 bilateral bending; **M.PB.**: maxilla canine pull-back **PM.2**: premaxilla anterior unilateral
580 bending; **PM.3**: premaxilla canine unilateral bending; **PM.PB.**: premaxilla canine pull-
581 back; **S.S.**: canine skull shake.

582

583 **Figure 5.** Von Mises stress contour plots from FEA of *Allosaurus fragilis* and *Alligator*
584 *mississippiensis* for the intrinsic scenarios. Mean von Mises values per scenario for each
585 taxon are displayed on the right. **JUMB.**: jaw unilateral muscle-driven bite; **SUMB.**:
586 skull unilateral muscle-driven bite.

587

588 **Figure 6.** Comparison of von Mises stress distribution for scaled models of different
589 archosaurian carnivores: baurusuchid, *Allosaurus fragilis* and *Alligator mississippiensis*.
590 Stress contour plots displayed for the anterior bending scenario. On the right,
591 comparative mean von Mises values per scenario for each taxon. **DAB.**: jaw anterior
592 bending; **DCB.**: jaw canine unilateral bending; **DPB.**: jaw canine unilateral bending;
593 **JBB.**: jaw canine bilateral bending; **MBB.**: maxilla canine bilateral bending; **MCB.**:
594 maxilla canine unilateral bending, **MPB**: maxilla posterior unilateral bending; **PMB.**:
595 unilateral premaxillary bending.

596

597 TABLES

598 **Table 1.** Selected measurements (in cm) for the skull LPRP/USP 0697

| **LPRP/USP 0697** | |
|---|---|
| Basal skull length (from tip of snout to occipital condyle along midline) | 33.10 |
| Length of skull (from posterior end of skull table to tip of snout, on midline) | 30.20 |
| Length of snout (from anterior end of orbit to tip of snout) | 18.27 |
| Greatest transverse width of skull (across quadratojugals) | 17.99 |
| Least transverse interorbital distance | 4.65 |
| Transverse width of skull at level of anterior ends of orbits | 7.13 |
| Transverse width of skull at level of postorbital bars | 9.59 |
| Transverse width of skull table anteriorly | 10.16 |
| Transverse width of skull table posteriorly | 15.23 |

599

600

601 **Table 2. Total force inferred from cranial and lower jaw attachments for each**

602 **muscle modeled.**

| Muscle | Total muscle force (N) |
|---|---|
| *m. adductor mandibulae externus medialis* | 132.65 |
| *m. adductor mandibulae externus profundus* | 227.625 |
| *m. adductor mandibulae externus superficialis* | 157.875 |
| *m. adductor mandibulae posterior* | 249.475 |
| *m. depressor mandibulae* | 245.925 |
| *m. intramandibularis* | 87.775 |
| *m. pseudotemporalis profundus* | 61.25 |
| *m. pterygoideus dorsalis* | 235.94 |
| *m. pterygoideus ventralis* | 198.4 |

603

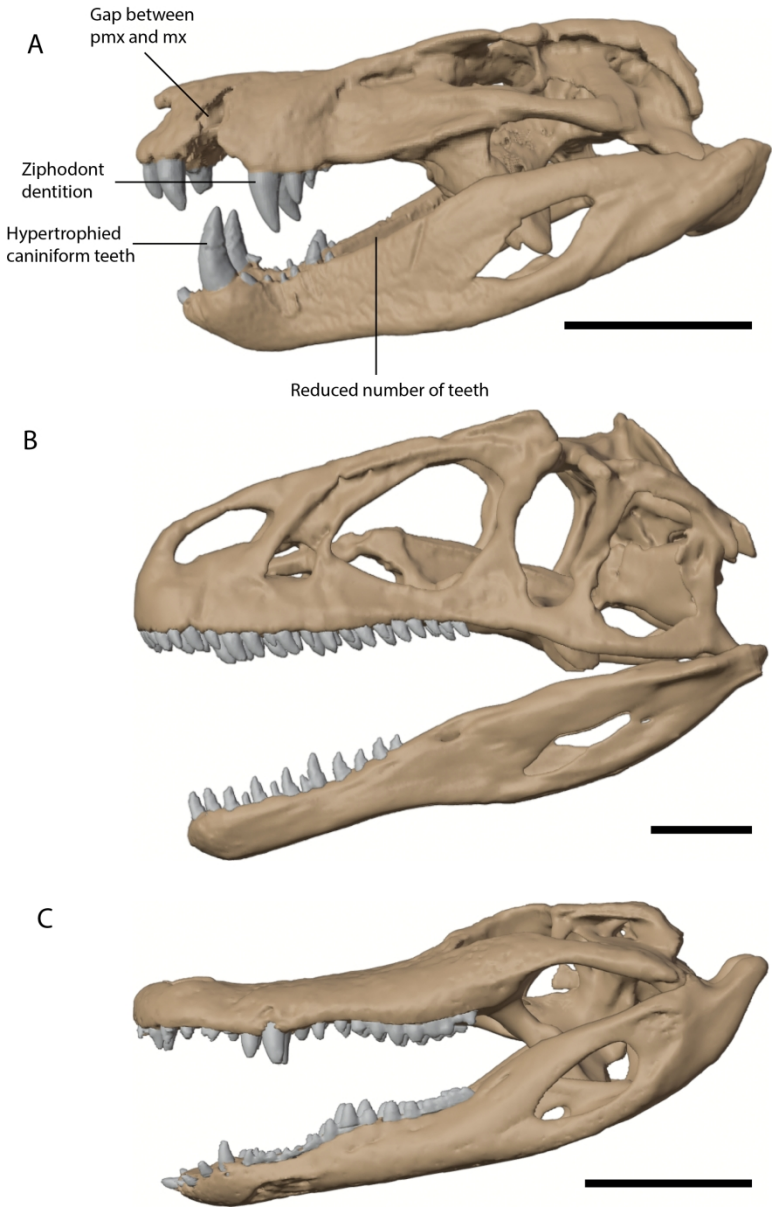


Figure 1. Digitally restored models of skulls used in this study. A- Baurusuchid (LPRP/USP 0697) in lateral view showing typical traits of the members of the clade. B- Allosaurus fragilis (MOR 693) in lateral view. C- Alligator mississippiensis (OUVC 9761) in lateral view.

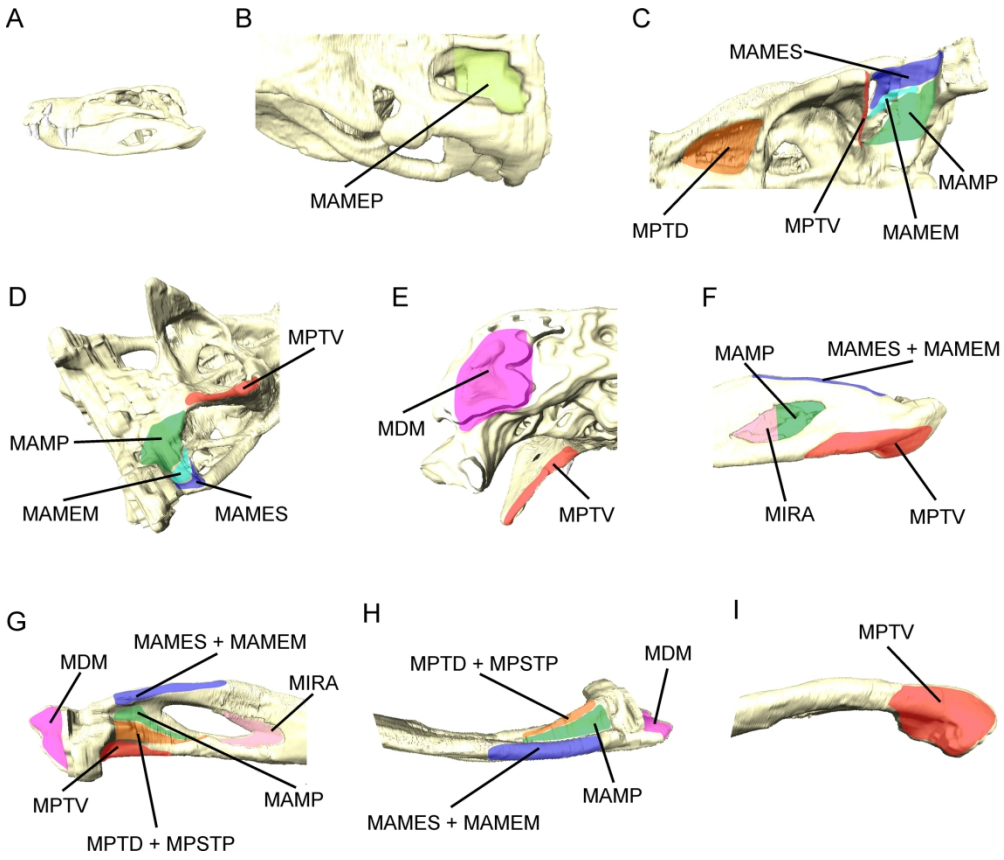


Figure 2. Muscle attachment areas plotted on the 3D model of skull the baurusuchid LPRP/USP 0697. A, skull and lower jaws in lateral view; B, dorsal view of the left posterior of the skull; C, ventral view of the left posterior of the skull; D, posterolateral view of the skull; E, occipital view of the left portion of the skull; F, lateral view of the posterior portion of the left mandibular ramus; G, medial view of the posterior portion of the left mandibular ramus; H, occlusal view of the posterior portion of the left mandibular ramus; I, ventral view of the posterior portion of the left mandibular ramus. MAMEM: m. adductor mandibulae externus medialis; MAMEP: m. adductor mandibulae externus profundus; MAMES: m. adductor mandibulae externus superficialis; MAMP: m. adductor mandibulae posterior; MDM: m. depressor mandibulae; MIRA: m. intramandibularis; MPSTPS: m. pseudotemporalis profundus; MPTD: m. pterygoideus dorsalis; MPTV: m. pterygoideus ventralis.

210x177mm (300 x 300 DPI)

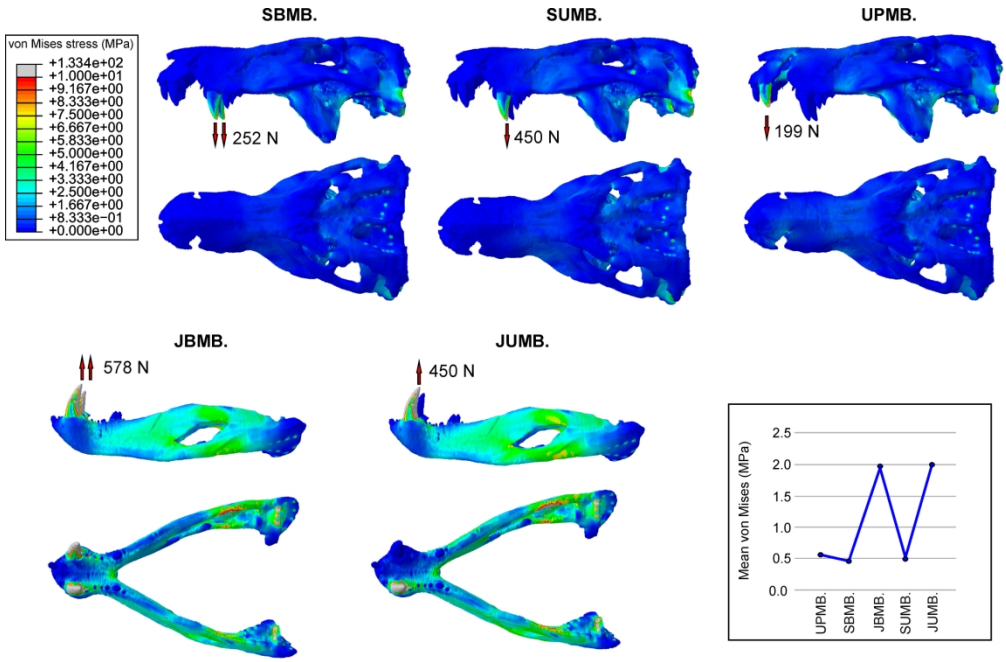


Figure 3. Von Mises stress contour plots from finite elements analysis (FEA) of the baurusuchid specimen (LPRP/USP 0697) for the intrinsic scenarios. Arrows indicate the location of muscle-driven bite forces on models during each scenario, with respective estimated bite force values. Mean von Mises values per scenario are displayed on the bottom right. JBMB.: jaw bilateral mucle-driven bite; JUMB.: jaw unilateral mucle-driven bite; SBMB.: skull bilateral muscle-driven bite; SUMB.; skull unilateral muscle-driven bite; UPMB.: unilateral premaxillary muscle-driven bite.

204x133mm (300 x 300 DPI)

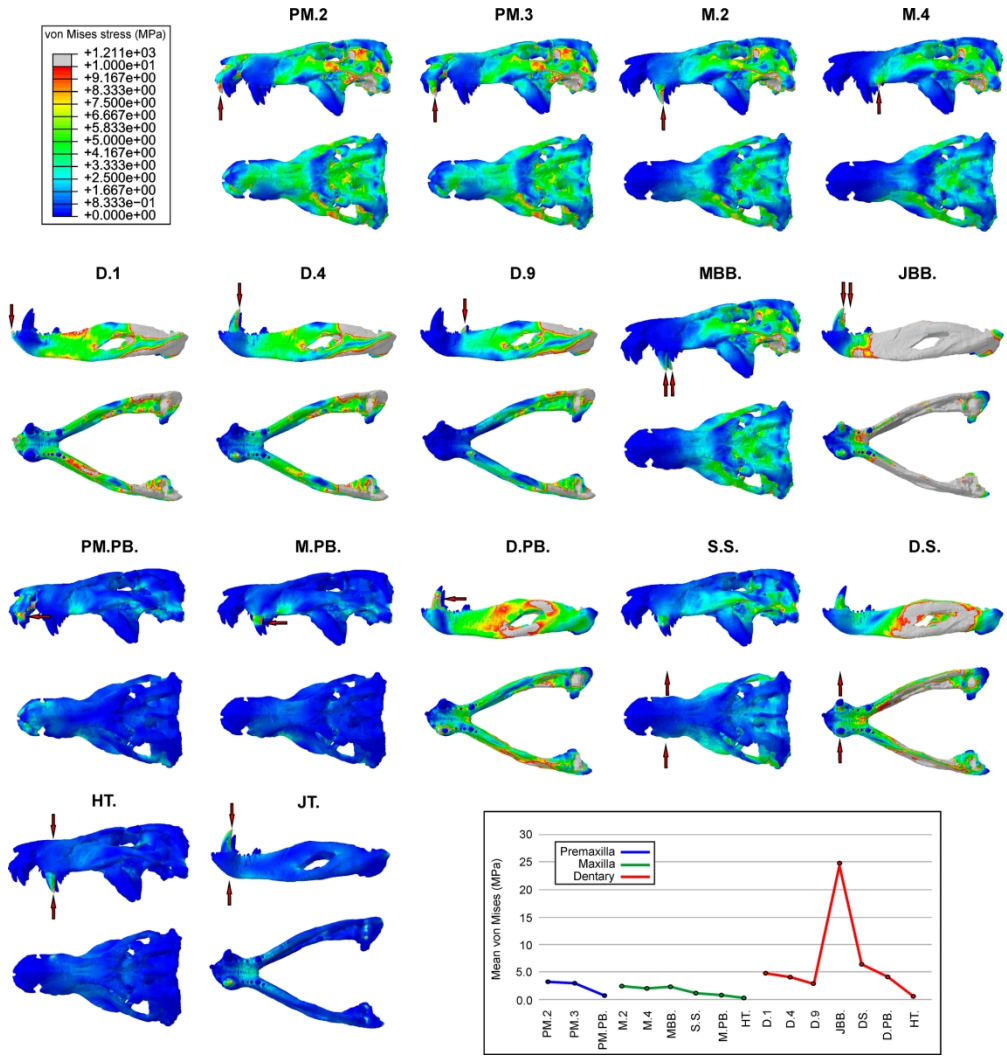


Figure 4. Von Mises stress contour plots from FEA of the baurusuchid specimen LPRP/USP 0697, comparing the stress distribution of skull and mandible models under distinct functional bending scenarios. Arrows indicate the location on the models of the loading vectors for each scenario. Mean von Mises values per scenario are displayed on the bottom right. D.1: jaw anterior unilateral bending; D.4: jaw canine unilateral bending; D.PB.: dentary canine pull-back; D.S.: canine dentary shake; HT.: head-twist (skull); JBB.: jaw canine bilateral bending; JT.: head-twist (jaw); M.2: maxilla canine unilateral bending; M.4: maxilla posterior unilateral bending; MBB.: maxilla canine bilateral bending; M.PB.: maxilla canine pull-back PM.2: premaxilla anterior unilateral bending; PM.3: premaxilla canine unilateral bending; PM.PB.: premaxilla canine pull-back; S.S.: canine skull shake.

210x220mm (300 x 300 DPI)

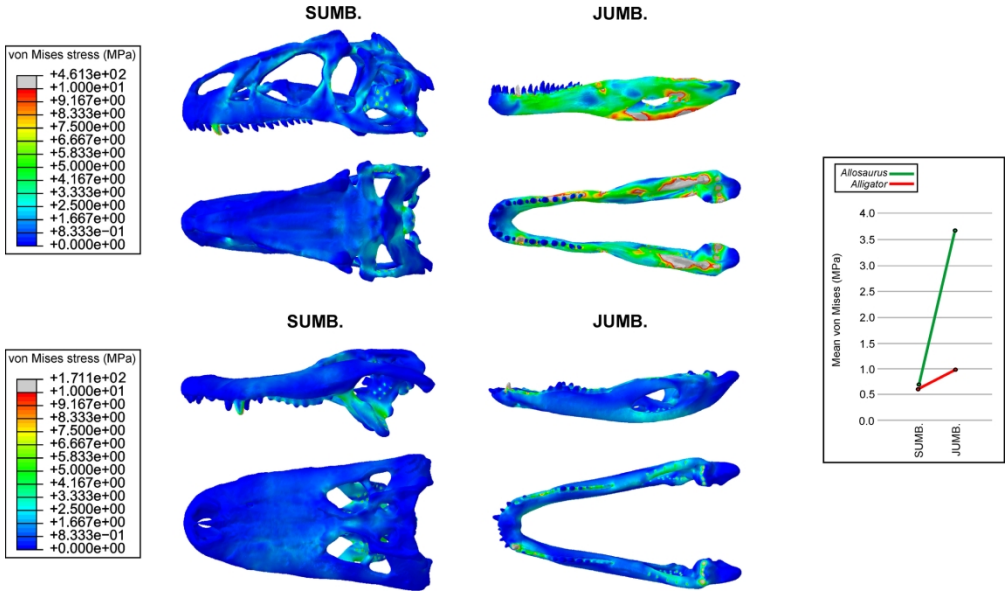


Figure 5. Von Mises stress contour plots from FEA of Allosaurus fragilis and Alligator mississippiensis for the intrinsic scenarios. Mean von Mises values per scenario for each taxon are displayed on the right. JUMB.: jaw unilateral muscle-driven bite; SUMB.: skull unilateral muscle-driven bite.

200x117mm (300 x 300 DPI)

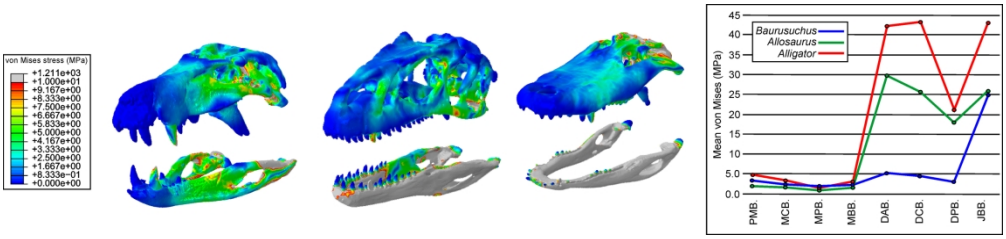


Figure 6. Comparison of von Mises stress distribution for scaled models of different archosaurian carnivores: baurusuchid, Allosaurus fragilis and Alligator mississippiensis. Stress contour plots displayed for the anterior bending scenario. On the right, comparative mean von Mises values per scenario for each taxon. DAB.: jaw anterior bending; DCB.: jaw canine unilateral bending; DPB.: jaw canine unilateral bending; JBB.: jaw canine bilateral bending; MBB.: maxilla canine bilateral bending; MCB.: maxilla canine unilateral bending, MPB: maxilla posterior unilateral bending; PMB.: unilateral premaxillary bending.

237x54mm (300 x 300 DPI)